

# Journal of Materials Chemistry B

Accepted Manuscript



This is an *Accepted Manuscript*, which has been through the Royal Society of Chemistry peer review process and has been accepted for publication.

*Accepted Manuscripts* are published online shortly after acceptance, before technical editing, formatting and proof reading. Using this free service, authors can make their results available to the community, in citable form, before we publish the edited article. We will replace this *Accepted Manuscript* with the edited and formatted *Advance Article* as soon as it is available.

You can find more information about *Accepted Manuscripts* in the [Information for Authors](#).

Please note that technical editing may introduce minor changes to the text and/or graphics, which may alter content. The journal's standard [Terms & Conditions](#) and the [Ethical guidelines](#) still apply. In no event shall the Royal Society of Chemistry be held responsible for any errors or omissions in this *Accepted Manuscript* or any consequences arising from the use of any information it contains.

# Bioactive glass-gelatin hybrids : building scaffolds with enhanced calcium incorporation and controlled porosity for bone regeneration

*Jonathan Lao<sup>\*§</sup>, Xavier Dieudonné<sup>§</sup>, Franck Fayon<sup>||</sup>, Valérie Montouillout<sup>||</sup>, and Edouard Jallot<sup>§</sup>.*

§ Clermont Université, Université Blaise Pascal, CNRS/IN2P3, Laboratoire de Physique Corpusculaire, BP 10448, F-63000 CLERMONT-FERRAND, France.

|| CNRS, CEMHTI UPR3079, Université d'Orléans, 1D avenue de la Recherche Scientifique, Orléans, 45071, France

\* Corresponding author: [lao@clermont.in2p3.fr](mailto:lao@clermont.in2p3.fr)

Keywords: Calcium silicate glass, organic-inorganic hybrid materials, scaffolds, bioactivity.

Abstract:

Thanks to their active promotion of bone formation, bioactive glasses (BG) offer unique properties for bone regeneration, but their brittleness prevents them from being used in a wide range of applications. Combining BG with polymers into a true hybrid system is therefore an ideal solution to associate toughness from the polymer and stimulation of bone mineralization from the glass. In this work, we report the synthesis and characterization of hybrid scaffolds based on SiO<sub>2</sub>-CaO bioactive glass and gelatin, a hydrolyzed form of bone type-I collagen. Incorporation of calcium ions, known to trigger bone formation and cellular activity, into the hybrid structure was achieved at ambient temperature through careful control of chemistry of the sol-gel process. Thorough characterization of the materials highlights the effect of grafting

an organoalkoxysilane coupling molecule to covalently link networks of BG and gelatin, and proves it a successful mean to take control over the degradation and bioactive properties of hybrids. Importantly, BG-gelatin hybrids are synthesized in a process fully conducted at ambient temperature that allows open-porous scaffolding structures to be obtained, with well-controlled and tuneable porosity regarding both pore and interconnection sizes. Mechanical properties of the scaffolds under compression are similar to trabecular bone and their apatite-forming ability is even higher than that of pure BG scaffold foams.

### 1. Introduction

For advanced engineering of bone tissues, it has been a constant concern to take advantage of the unique properties of bioactive glasses (BG) to build scaffolding materials able to guide bone ingrowth.<sup>1</sup> BG are known to efficiently stimulate bone regeneration<sup>2</sup>, being even able to bond to soft tissues. However, their brittleness is a serious drawback, and prevents them from sharing mechanical load with bone. Composite materials consisting of BG particles dispersed in a bioresorbable polymer matrix show improved mechanical properties, but the absence of interfacial bonding between the organic and inorganic components, which usually have very different degradation rates, can cause instability and premature deterioration of the scaffold<sup>3</sup>. On the contrary, hybrid materials have the key advantage of behaving as a single phase, due to their interpenetrated organic–inorganic networks interacting at the molecular level<sup>4</sup>. Thereby, the development of BG-based hybrids exhibiting high bioactivity, toughness and controlled congruent degradation has become a priority interest.

Until now, the main hindrance to the development of bioactive hybrid scaffolds was related to the difficulty of incorporating calcium ions into the BG silicate network. Calcium plays a major role in osteogenesis and has a beneficial effect on osteoblast proliferation, differentiation, and mineralization of the extracellular matrix<sup>5</sup>. Indeed bone cells own specific receptors that are activated in the presence of calcium ions, and that govern the expression of growth factors<sup>6</sup>. In the common sol-gel synthesis of BG, calcium is introduced using metal

salts like  $\text{CaCl}_2$  or  $\text{Ca}(\text{NO}_3)_2$  and the incorporation of the calcium as modifier cation in the silicate network require thermal treatments above  $400^\circ\text{C}$ .<sup>7</sup> Such thermal treatments are not compatible with the synthesis of BG-polymer hybrids, therefore in the literature most syntheses conducted at low temperature lead to pure silica-polymer hybrids with heterogeneous calcium deposits outside the silicate network.<sup>8-10</sup> These calcium deposits can be washed out at the first contact with biological fluids, causing a severe alkaline shock and a sudden pH raise which can result in fibrous encapsulation of the implant or even more serious complications *in vivo*.<sup>5,11</sup> An alternative way allowing calcium incorporation into the inorganic part of the hybrid at room temperature is the use of calcium alkoxides as precursors. However, its high sensitivity towards hydrolysis–condensation reactions in the presence of water<sup>12,13</sup> can give rise to premature gelation of the sol raising the question of homogeneity of the obtained scaffold,<sup>14</sup> and making it impossible to handle the hybrid sol for tailoring the desired macroporous shapes of the implant. Thus, it is worth noting that the so-called BG-hybrids reported in the literature either do not incorporate calcium<sup>8,9,15-18</sup>, or cannot be processed to give the suitable form of scaffolds, being produced in the form of dense<sup>19</sup> or fiber materials<sup>14</sup>.

The aim of our study was to develop a new protocol that would allow the easy synthesis of BG hybrid scaffolds with tailored properties, based on  $\text{SiO}_2$ -CaO BG, a simple and known bioactive composition<sup>20</sup>, and gelatin, a suitable and inexpensive hydrolyzed form of bone type I collagen<sup>21</sup>. In a previous work<sup>22</sup> we reported enhanced calcium incorporation and organic-inorganic interfacial bonding inside  $\text{SiO}_2$ -CaO/gelatin hybrids. However hybrids were synthesized in the form of powder. Processing it to obtain scaffolds is challenging since thermal treatments are to be banished to preserve the organic component. Here we found a convenient way of introducing tailored porosity inside BG-gelatin hybrids, being achieved at ambient temperature. Important added benefits are the ease of use of our protocol, its

versatility, the safety of employed reactants, solvents and generated by-products, and its inexpensive cost.

## 2. Results and Discussion

### 2.1. BG-gelatin hybrid scaffolds synthesis

To overcome the difficulties mentioned above regarding the introduction of calcium alkoxides in the sol-gel process and their extreme reactivity to water, one of the key is to limit the introduction of water in the sol to achieve convenient slow-down of the gelation process. In this work, we used the calcium alkoxide precursor in dilute conditions (7 wt.% ratio). Calcium ethoxide ( $\text{Ca}(\text{OEt})_2$ ) was chosen as the calcium source, rather than calcium methoxyethoxide used in pioneer studies,<sup>12-14, 23</sup> because of the safety of the by-product generated (ethanol here, while methanol by-products can be generated in the above references). This is of special importance in case of incomplete hydrolysis of the alkoxide since the remaining ligands are likely to be released *in vivo*. In our synthesis route, tetraethylorthosilicate (TEOS) is first hydrolysed in a slightly acidified alcoholic solution and then mixed with  $\text{Ca}(\text{OEt})_2$  to form the inorganic glass silicate network. The proportions of Si and Ca alkoxides are adjusted to obtain a 75 wt. %  $\text{SiO}_2$ -25 wt.% CaO BG composition known to induce rapid bioactivity.<sup>24</sup> In parallel, a polymer solution is prepared. Gelatin appears as an appropriate polymer component as it derives from bone type I collagen (90 % of bone organic matter)<sup>25</sup> but without expressing antigenicity in physiological conditions.<sup>26</sup> Binding sites are available for cell attachment and gelatin can be degraded enzymatically through a cell-mediated process<sup>21</sup> in. This potentially results in a more linear degradation rate *in vivo*<sup>27</sup> than the autocatalytic chain scission degradation of commonly used resorbable polyesters. Synthetic polymers also often require organic solvents or toxic initiators of polymerization, which can adversely affect interaction with cells<sup>28</sup>. For the synthesis of class-II hybrids with covalent linkage between the organic and inorganic networks, gelatin is functionalized with 3-glycidoxypropyltrimethoxysilane (GPTMS) as coupling agent. After

hydrolysis of the GPTMS methoxysilane groups, the polymer solution is added to the sol to undergo condensation with the silanol groups of the glass oligomeric species. For both raw and functionalized gelatin, polymerization of the hybrid network typically occurs within 2 hours, allowing convenient handling of the sol and shaping process.

3D-interconnected macroporous hybrid structures with well-controlled pore diameters and interconnections are obtained using the microsphere-leaching technique up to a 50 wt.% BG fraction. In brief, the hybrid sol is infiltrated into a compact stack of PMMA microspheres. After gelation of the hybrid, the PMMA porogen spheres are dissolved in acetone, leaving a highly porous hybrid structure with well-controlled pore diameters and interconnections.

**Figure 1** and Fig. S1 shows the variety of macroporous structures indifferently obtained for class I or class II BG hybrid scaffolds (without or with covalent linkages between organic–inorganic networks through GPTMS coupling, respectively). For successful bone ingrowth and vascularisation it is generally admitted that the minimum pore size should be  $100\ \mu\text{m}$ <sup>29</sup>, while enhanced bone regeneration and formation of capillaries are reported for pores larger than  $200\text{--}300\ \mu\text{m}$  and interconnections superior to  $50\ \mu\text{m}$ <sup>30</sup>. The scaffold porosity can be readily adjusted to these specifications, as it directly depends on the size distributions of the PMMA porogen microspheres. The distribution of pore diameters nicely follows the granulometric distribution of the porogen spheres while the interconnection sizes depend on the size of the contact point between each porogen spheres in the initial stack.<sup>31</sup> The interdependence of these two parameters has been investigated for a variety of granulometric distributions of the PMMA porogen spheres ( $100\text{--}200\ \mu\text{m}$ ,  $200\text{--}300\ \mu\text{m}$ ,  $200\text{--}400\ \mu\text{m}$ ,  $300\text{--}500\ \mu\text{m}$ ,  $400\text{--}1000\ \mu\text{m}$  diameter ranges). Fig.1-d shows a linear relationship between these parameters, highlighting the ability to build hybrid scaffolds with finely-tuned macroporosity designed for a particular application. Additionally, the interconnection sizes can even be easily increased, since the contact points between each porogen microspheres of the PMMA template can be enlarged by infiltrating acetone or by thermal treatment, causing partial

dissolution and bridging of the spheres.<sup>32</sup> Fig. 1-e and 1-f show how interconnections size distributions can be efficiently modulated using these techniques. Since the size of interconnections is one of the determinant parameters for bone regeneration – “no bone without vasculature”<sup>33</sup> – the ability to finely tune their distributions is key and should even allow a fine control over the regulation of osteogenesis. As an example Fig.1-d illustrates the widening of the interconnections when microspheres are bridged together for 30 minutes using a 30 wt.% acetone solution before infiltration of the hybrid sol.

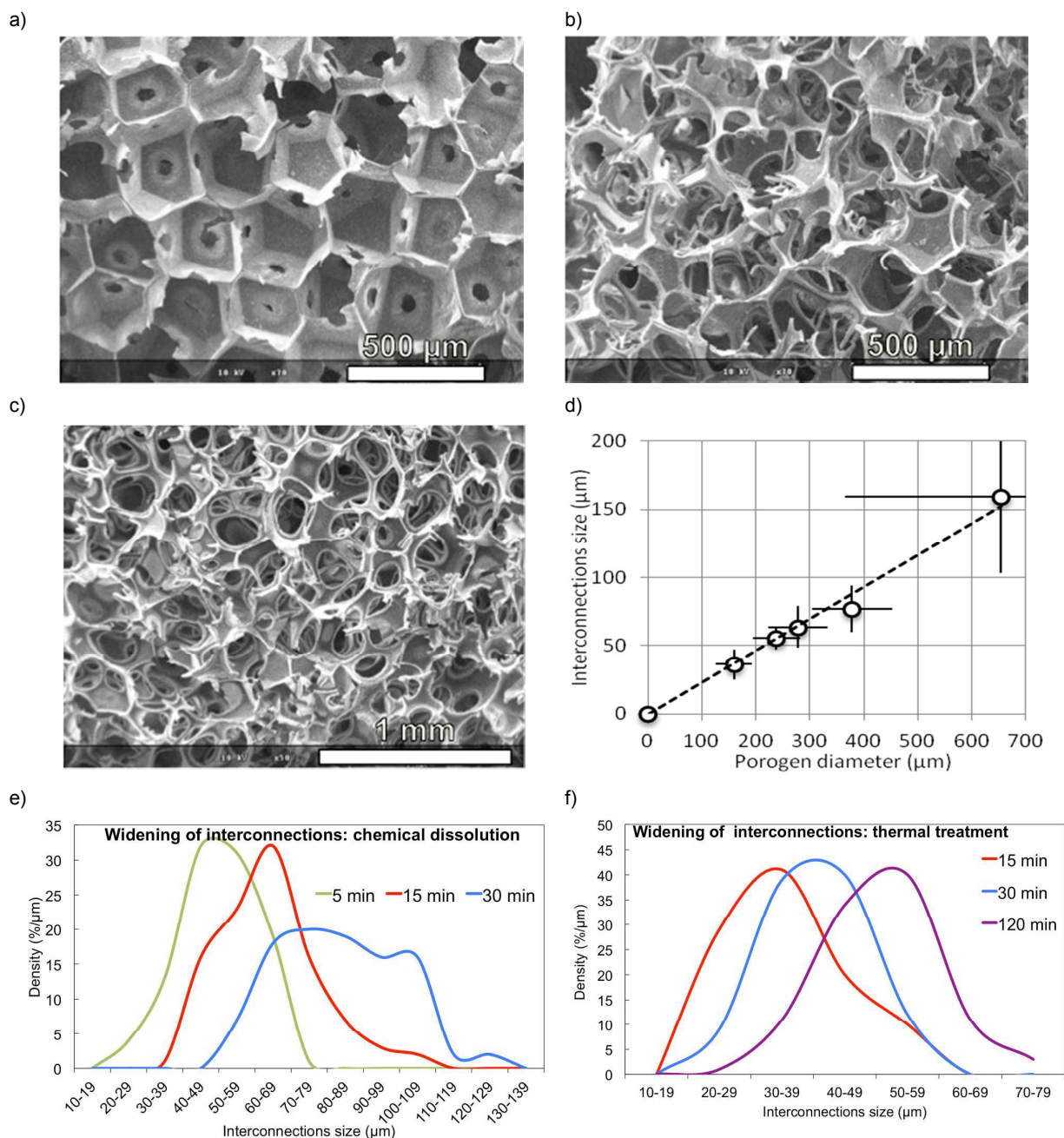
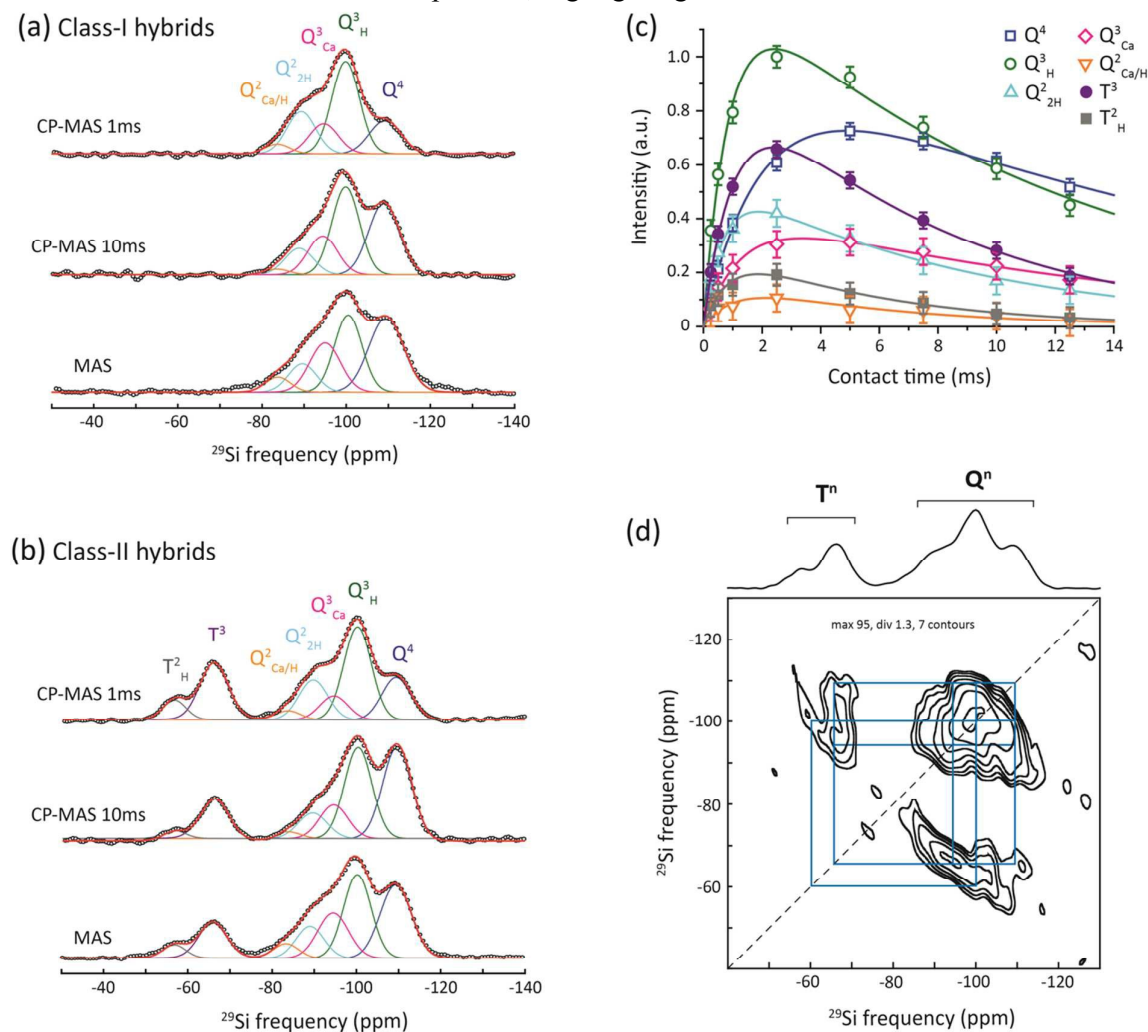


**Figure 1. Examples of bioactive glass-gelatin hybrid scaffold microstructures with controlled pore and interconnection sizes.** SEM image of cross sections of (a) a class-II BG hybrid scaffold (30wt.%  $\text{SiO}_2\text{-CaO}$ /70 wt.% gelatin) with a selective distribution of pore size in the 200–400  $\mu\text{m}$  range. (b) Widening of the interconnections by increasing the contact point of porogen spheres in the PMMA template used for (a) through partial chemical dissolution of the spheres. Note that the pore size distribution in the 200–400  $\mu\text{m}$  range is preserved. (c) Same structure obtained inside class-II BG/gelatin hybrid scaffolds with 50 wt.%  $\text{SiO}_2\text{-CaO}$  / 50 wt.% gelatin. (d) Variation of the mean interconnections size as a function of the average porogen diameter (i.e. equivalent to pore diameter) for different granulometric distributions of the porogen spheres, showing a linear relationship between the two parameters. Error bars correspond to standard deviation. (e) Number distributions of interconnections size obtained when the contact point of porogen spheres in the PMMA template is increased by chemical dissolution using a 30 wt.% acetone solution for varying times. PMMA porogen spheres had diameters in the 100–300  $\mu\text{m}$  range. (f) Number distributions of interconnections size obtained when the contact point of porogen spheres in the PMMA template is increased by pre-heating at 125°C for different times. PMMA porogen spheres had diameters in the 100–300  $\mu\text{m}$  range.

## 2.2. Investigation of calcium incorporation and organic-inorganic covalent linking

Calcium incorporation inside class I and class II hybrids can be investigated from the distribution of  $Q^n$  species in the silicate network which can be obtained through NMR.  $Q^n$  species call for  $[SiO_4]$  units with  $n$  bridging oxygens, and thus  $(4-n)$  non bridging oxygens. The latter are created when residual silanols are present and/or network modifiers such as calcium ions are incorporated. Here the disordered structures of the synthesized class-I and -II hybrid scaffolds were probed by  $\{^1H\}$ - $^{29}Si$  cross-polarization (CP) magic angle spinning (MAS) NMR. For short CP durations, these experiments allow to selectively enhance the signals of silanol units, while the resonances of Si units far from hydrogen atoms are amplified for longer CP times.<sup>34</sup> As shown in **Figure 2**, the obtained spectra give evidence for the presence of several partly overlapping resonances associated to distinct  $Q^n$  units. Good fits of the CP MAS spectra, which account for the lineshape modifications observed as a function of the CP time (Figure S2 and S3), are obtained considering five individual contributions in the -75 to -120 ppm frequency range. According to the  $^{29}Si$  isotropic chemical shift ranges,<sup>34, 35</sup> these peaks located at -109.5, -100, -94.7, -90.5 and -83.5 ppm are assigned to  $Q^4$ ,  $Q^3_H$ ,  $Q^3_{Ca}$ ,  $Q^2_{2H}$  and  $Q^2_{Ca/H}$  units, respectively. This assignment is also consistent with the CP time constants ( $T_{SiH}$ ) determined from the intensity variations of each individual resonance as a function of the CP time (Figure 2c and S4). Short  $T_{SiH}$  values of about 0.75 and 0.6 ms are found for  $Q^3_H$  and  $Q^2_{2H}$  silanol groups, respectively, while the  $Q^4$  and  $Q^3_{Ca}$  units (with weaker Si-H dipolar couplings) exhibits significantly longer  $T_{SiH}$  of 1.9 and 1.2 ms (**Table S1**). On this basis, analysis of the quantitative  $^{29}Si$  MAS spectra reveals that a significant amount of Ca atoms disrupts the siloxane bridging oxygen bonds and thus effectively takes part in the BG network formation, as evidenced by the intensities of  $Q^3_{Ca}$  and  $Q^2_{Ca/H}$  resonances measured for both class I and class II hybrids as shown in Table S1.

**Figure 2. Structural characterization of the hybrid scaffolds.** Experimental  $^{29}\text{Si}$  CP MAS and MAS NMR spectra (black dots) of (a) class-I and (b) class-II hybrid scaffolds (50 wt.%  $\text{SiO}_2\text{-CaO}$  BG /50 wt.% gelatin) and their fits (red lines). In (a) and (b), top and middle correspond to the CP MAS spectra recorded with CP durations of 1 and 10 ms, respectively, and bottom is the quantitative MAS spectrum. Individual  $\text{Q}^n$  and  $\text{T}^n$  contributions are shown below each experimental spectrum. (c) Variation of the individual  $\text{Q}^n$  and  $\text{T}^n$  resonances as a function of the CP duration. Open and filled symbols correspond to  $\text{Q}^n$  and  $\text{T}^n$  resonances, respectively. The curves correspond to fits of the data points using the expression  $I(t) = I_0(1 - T_{\text{SiH}}/T_{1\rho}^{\text{H}})^{-1}[\exp(-t/T_{1\rho}^{\text{H}}) - \exp(-t/T_{\text{SiH}})]$ , where  $T_{\text{SiH}}$  is the CP time constant and  $T_{1\rho}^{\text{H}}$  is the  $^1\text{H}$  spin-lock longitudinal relaxation constant (d) Sheared 2D  $^{29}\text{Si}$  dipolar DQ-SQ correlation spectrum. The diagonal of the spectrum is shown as the dotted black line. The blue lines indicate the cross-correlation patterns, highlighting the Si-O-Si connectivities.



In addition to the resonance of the  $Q^n$  units, the  $^{29}\text{Si}$  MAS and CP MAS spectra of the class-II BG-gelatin hybrids exhibit two peaks characteristic of  $T^n$  units ( $\text{SiO}_3\text{C}$  unit with  $n$  bridging oxygen atoms) resulting from the hydrolysis/condensation of the terminal methoxysilane groups of GPTMS.  $T^n$  species are present for organoalkoxysilane molecules. GPTMS, either hydrolysed or not, is characterized by  $T^0$  units due to its three terminal trimethoxysilane chains (or terminal silanols if hydrolysed). If condensation of the terminal chains occurs to form bridging  $\text{C}-\underset{\text{|}}{\overset{\text{|}}{\text{Si}}}-\text{O}-\text{Si}\text{---}$  bonds, then  $T^1$ ,  $T^2$  and  $T^3$  units would appear and indicate either a successful GPTMS grafting onto the inorganic silicate network, or GPTMS autocondensation. Here, according to their  $^{29}\text{Si}$  isotropic chemical shifts, the two resonances observed are assigned to  $T^3$  (-66.0 ppm) and  $T^2$  (-56.8 ppm) units. The amount of linkage between the BG silicate network and these terminal groups of the GPTMS chains grafted onto gelatin was investigated using  $^{29}\text{Si}$  two-dimensional (2D) homonuclear dipolar double quantum –single quantum (DQ-SQ) MAS correlation experiment. With adjusted experimental conditions, it allows to selectively probe the short-range Si-Si interatomic proximities reflecting directly the Si-O-Si connectivities. Connectivities between distinct Si units are revealed by paired cross-correlation peaks while the presence of linkages between equivalent Si units is disclosed by an auto-correlation peak located on the diagonal of the 2D spectrum. As shown in figure 2d, the obtained 2D DQ-SQ correlation spectrum nicely reveals the connectivities between the  $Q^n$  units forming the BG network. More importantly, covalent bonding between GPTMS chains and the BG silicate network is clearly evidenced by  $T^n$ - $Q^n$  cross-correlation peaks and the absence of auto-correlation peak between  $T^n$  units indicates that polycondensation between GPTMS chains does not occur. This shows unambiguously that GPTMS is successfully grafted to the BG network, ensuring the efficient coupling between the organic and inorganic part of the hybrid network.

### 2.3. Congruent degradation, thermal behaviour, increased mechanical properties

The crosslinking of the organic and inorganic parts of the hybrid network using GPMTS as coupling agent gives rise to enhanced properties of class-II hybrids scaffolds. **Figure 3-a** compares the degradation rates of class I and class II BG-gelatin hybrids (30 wt.% SiO<sub>2</sub>-CaO BG/70 wt.% gelatin) when immersed in Simulated Body Fluids (SBF) at 37°C. The observed synchronic Si and gelatin release curves indicate that both class I and class II hybrids undergo congruent dissolution, due to the extended inner interface between their organic and inorganic networks. It should be noted that the dissolution products of the glass triggers the formation of bone mineral (apatite crystals) by changing the local supersaturation of the medium with respect to apatite precipitation,<sup>36,37</sup> while ionic species not directly involved in the mineralization process (like Si ions) are eliminated through natural excretion routes.<sup>20,38</sup>

For class-I hybrid, in which only weak interactions (hydrogen bonds and van der Waals interactions) between the gelatin chains and the BG network occur, a significant release of gelatin and Si ions is observed after 3 days of immersion, with average gelatin and Si concentration of 33 and 47ppm measured in the fluid. For class II hybrid with the same BG/gelatin ratio, the gelatin and Si releases are both much lower with only 10 and 22 ppm of gelatin and Si measured after 3 days of immersion. This can be obviously attributed to the stronger interactions between the organic and inorganic chains; indeed from the NMR study and Table S1 it was clear that class I and class II hybrids had similar disordered structures from their distribution of Q<sup>n</sup> units which are nearly identical. Silicate network connectivity can be calculated using the formula<sup>17</sup>  $NC = 1/3(2T^2+3T^3) + 1/4(2Q^2+3Q^3+4Q^4)$  and based on Table S1 it yields the same value (80% silicate network connectivity) for both class I and class II hybrids. However, the presence of T<sup>n</sup> species implies that in the gelatin network of class II hybrids, a significant number of hydrogen bonds are replaced by strong covalent bonds due to GPTMS grafting. This was confirmed with Differential Scanning Calorimetry

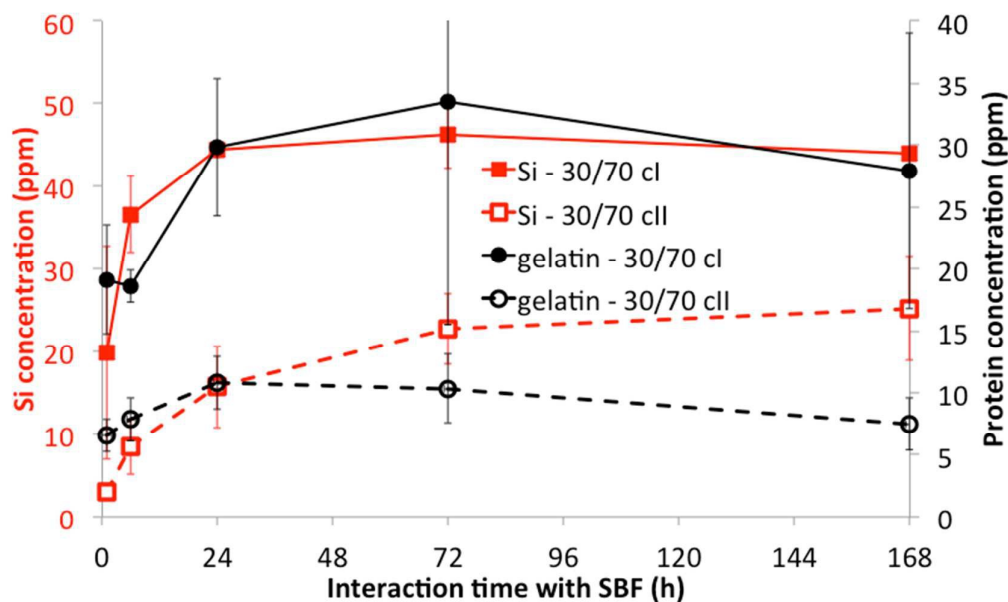
measurements: Figure 4-a shows there is an increase in the glass transition temperature of gelatin for class II hybrids ( $T_g = 74^\circ\text{C}$ ) with respect to class I ( $T_g = 68^\circ\text{C}$ ). Moreover at higher temperatures (ca.  $150^\circ\text{C}$ ), gelatins are often characterized by a first-order large endothermic transition which is attributed to the isomerization of the peptide bonds that constitute the polyproline-II helices of gelatin from the low energy *trans* to the high energy *cis* configuration.<sup>39</sup> The temperature of this isomerization peak increases ( $T_i = 163^\circ\text{C}$ ) for class II gelatin hybrids compared to class I ( $T_i = 129^\circ\text{C}$ ), indicating that more energy is needed to rearrange molecules, presumably due to the extent of covalent bonding and crosslinking in the gelatin network of class II hybrids. TGA thermograms (Figure 4-b) confirm these findings and demonstrate that class II hybrids are more resistant to thermal decomposition. The thermal decomposition of BG/gelatin hybrids consists of 2 steps, one below  $200^\circ\text{C}$  and the other one above  $200^\circ\text{C}$ , each of them resulting from the individual contribution of the gelatin and BG decomposition. To better understand this, we performed the TG analysis of pure gelatin and pure  $\text{SiO}_2\text{-CaO}$  sol-gel BG (see Figure S5). Thermogram of type B gelatin first consists of a dehydration process, ending at ca.  $100^\circ\text{C}$  and resulting here in a 16 wt% loss. Then the thermal decomposition of gelatin occurs, beginning at around  $275^\circ\text{C}$ , and resulting in a total weight loss of 83 wt% at  $850^\circ\text{C}$ . For the  $\text{SiO}_2\text{-CaO}$  BG, we also observe a 2 steps process, with first the removal of free water and silanol-bonded water, ending at around  $200^\circ\text{C}$  and causing a 10 wt% loss. It is immediately followed by a broad region of weight loss, corresponding to the dehydroxylation of Si-OH surface groups<sup>40</sup>, causing a total weight loss of 31 wt%. Hence we can hypothesize that a physical mixture of 30 wt%  $\text{SiO}_2\text{-CaO}$  BG with 70 wt% type B gelatin would undergo a 14 wt% weighted average loss at  $200^\circ\text{C}$ , and a total weighted average loss of 67 wt% above  $800^\circ\text{C}$ . These values have to be compared with those measured for BG/gelatin hybrids. Class I hybrids undergo a 13,5 wt% loss at  $200^\circ\text{C}$  and a 70 wt% total weight loss at  $850^\circ\text{C}$ , close to the hypothesized values of a simple physical mixture. For class II hybrids, the measured weight

losses are lower. There is a 9 wt% loss at 200°C, indicating that less water has been adsorbed in class II hybrids; indeed part of the silanols Si-OH groups have been substituted by siloxane Si-O-Si bonds as a result of GPTMS grafting, therefore providing less sites for water adsorption. Total weight loss is only 63 wt% at 850°C, lower than the hypothesized value, which can be explained here again by the lower quantities of silanols available for dehydroxylation.

The organic-inorganic crosslinking therefore results in a higher resistance of class II hybrid scaffolds towards dissolution and this improved chemical stability allows maintaining the mechanical properties after immersion. We found that class I hybrid scaffolds with 90% porosity showed poor compressive strength (1 kPa at 10 % deformation) after being immersed in physiological fluids, while class II BG-gelatin hybrids with 90 % porosity maintained satisfying properties even in a wet state, with compressive strength values two orders of magnitude higher than those of class I hybrids (108 kPa at 10 % deformation). Moreover, the measured decreases of calcium and phosphorus concentrations in SBF indicates that, although much more enduring to dissolution, class II hybrids showed bioactivity almost similar to that of class I materials. With respect to class I materials, class II hybrids appear thus suitable for a much broader range of applications and a deeper characterisation of their properties is described in the following.

**Figure 3. Dissolution products from class I and class II BG hybrid scaffolds (30wt.% SiO<sub>2</sub>-CaO/70 wt.% gelatin) released in Simulated Body Fluids. Variations of (a) Si and gelatin concentrations and (b) Ca and P concentrations as a function of interaction time with SBF.**

(a)



(b)

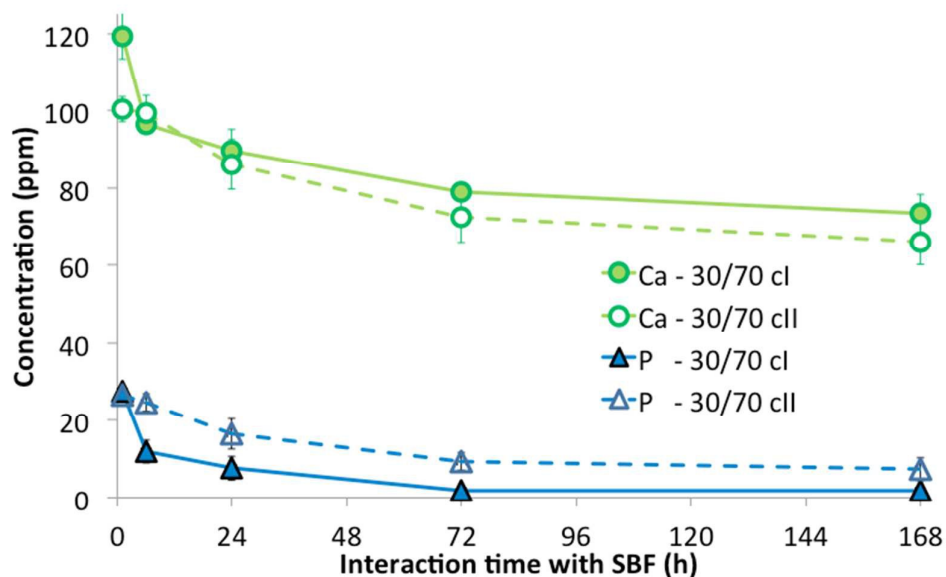
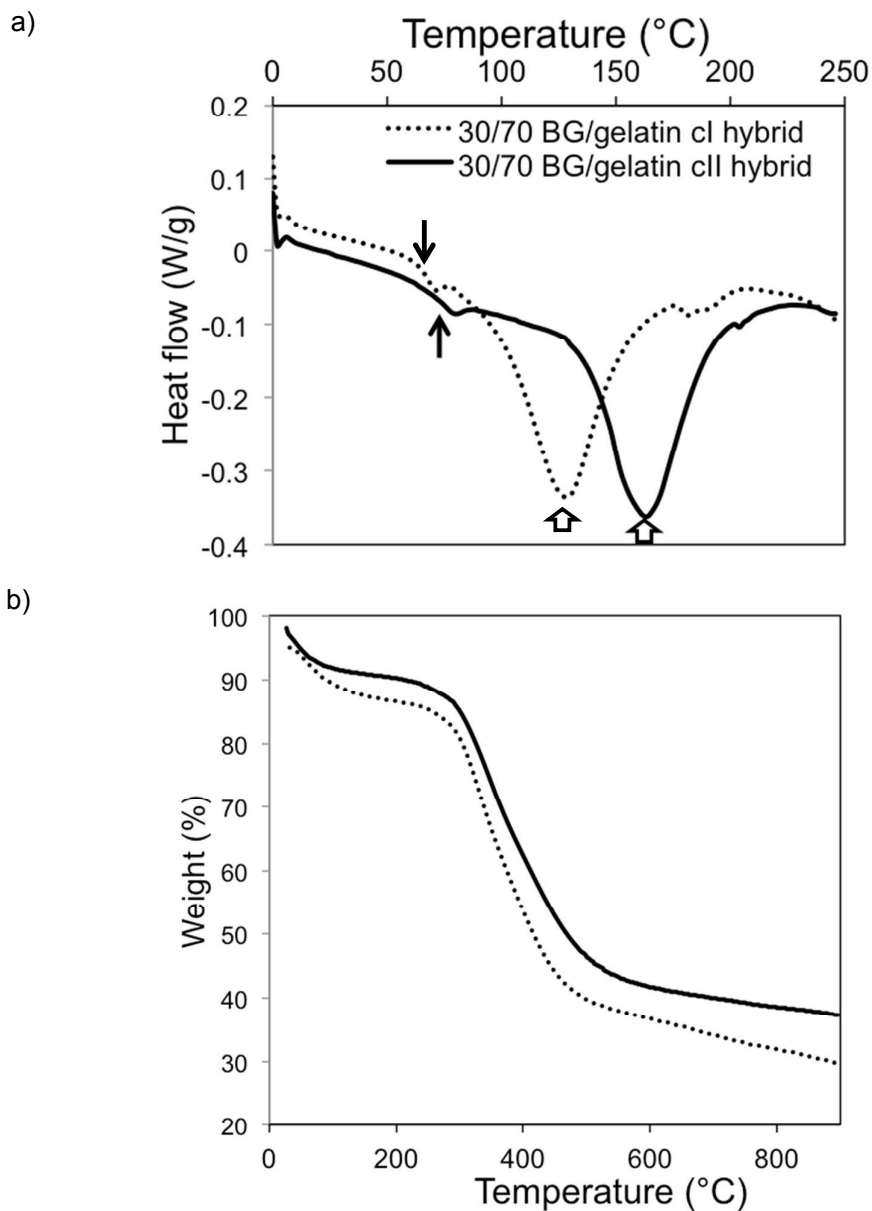
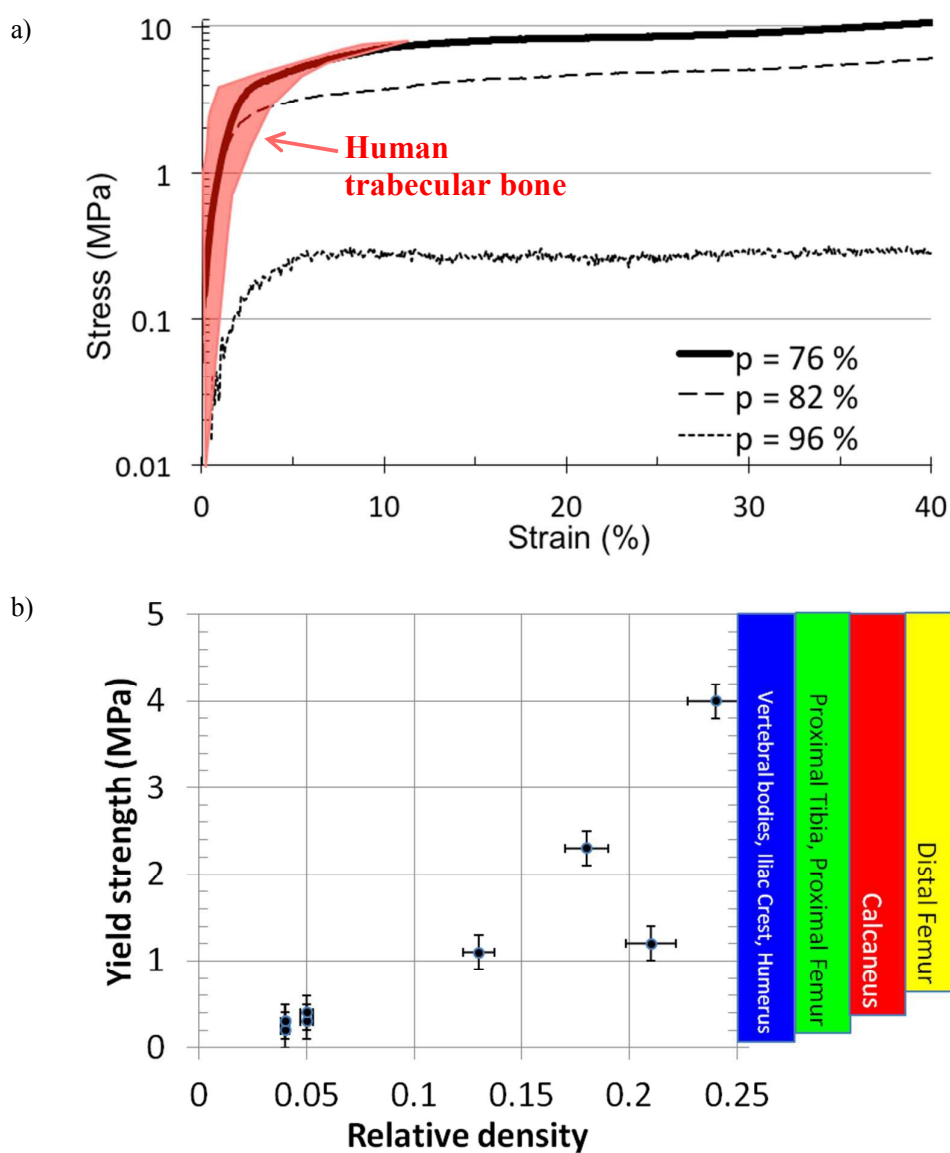


**Figure 4. a)** DSC heat flow normalized to unit mass for class I and class II BG/gelatin hybrids (30wt.% SiO<sub>2</sub>-CaO/70 wt.% gelatin). Thin arrows indicate glass transition T<sub>g</sub>, large plain arrows indicate position of isomerisation peak T<sub>i</sub>. **b)** Thermogravimetric analysis of BG/gelatin hybrids (30wt.% SiO<sub>2</sub>-CaO/70 wt.% gelatin).



The mechanical properties under compression were measured for class-II hybrid scaffolds with different porosities (from 76 % up to 96 % by varying the volume fraction of 100–400  $\mu\text{m}$  PMMA porogen). The obtained stress–strain curves are typical of elastomeric and elastic–plastic cellular solids<sup>41</sup> and are characterized by three regimes (**Figure 5-a**): a linear elastic regime corresponding to the cell edge bending, a stress plateau corresponding to progressive collapse of the macropores, and a final region of densification once total collapse of the pores throughout the material has occurred (this final region is not shown in Fig. 5-a). The yield strength at 0.2% offset and the Young modulus, which are known to decrease with increasing porosity,<sup>42</sup> are determined from the linear elastic regime. For porosities varying from 96 to 76 %, a concomitant increase of measured yield strength values from 0.3 up to 4 MPa (Figure 5-b) and of Young modulus from 5 to 166 MPa is observed. These values are among the highest ones reported in the literature for bioactive scaffolds (pure sintered glass scaffolds, sintered calcium phosphates or either polymer composites) with the same range of porosity (76%–96%).<sup>43, 44</sup> Compared to these materials, class-II gelatin–BG hybrids do not exhibit the brittle crushing of the pore walls in the plastic deformation regime, as demonstrated by the sustained value of the compressive strength in the stress plateau region of Fig.5-a. It should be noted that the yield strength values of these class-II hybrid scaffolds are similar to the ones reported for trabecular bones with the same porosity (corresponding to a relative density of 0.1 to 0.2), for which yield strength ranging from 0.2 to 4 MPa are reported (Figure 5-b).<sup>45, 46</sup> In particular, they are close to those of human tibial plateau or human calcanei.<sup>41, 47</sup> Despite the thinness of the scaffold pore walls ( $< 5 \mu\text{m}$ ), very satisfying properties are thus obtained and it is expected that these mechanical properties under compression can be further enhanced by increasing the thickness of the walls.

**Figure 5.** a) Stress–strain curves under compression obtained for class II BG-gelatin hybrid scaffolds (30wt.% SiO<sub>2</sub>–CaO/70 wt.% gelatin) with various porosity  $p$ . Typical response of human trabecular bone is indicated by the red shaded area (data from references <sup>45, 46, 48</sup>). b) Evolution of the yield strength at 0.2 % offset with relative density of class II BG hybrid scaffolds (30wt.% SiO<sub>2</sub>–CaO/70 wt.% gelatin). Color bars at the right represent the typical range of values reported for human trabecular bones from different anatomic locations (data from <sup>49</sup>)



#### 2.4. Extended apatite-forming ability, biocompatibility

The bioactivity of class II hybrid scaffolds was also characterized *in vitro* by immersion in Simulated Body Fluid (SBF) for varying periods, following the ISO-23317 recommendations.

**Figure 6** shows the cross-section of a hybrid scaffold after 3 days of interaction with SBF.

Advanced quantitative chemical imaging of the cross-section using PIXE nuclear microprobe reveals the very high bioactivity of class II hybrid scaffolds consisting of 30 wt.% SiO<sub>2</sub>-CaO / 70 wt.% gelatin. After interaction with SBF, the walls of the hybrid scaffold, which contain only little amounts of remaining Si (2.8 wt.%), are almost entirely changed into calcium phosphates having a Ca/P ratio close to that of biological apatites found in bone<sup>50</sup>. TEM observations plainly confirm needle-like agglomerates are observed *throughout* the scaffold sections after 3 days soaking in SBF (Fig. 6-e). The corresponding electron diffraction pattern (Fig. 6-f) is characteristic of hexagonal hydroxyapatite (HA) nanocrystals smaller than 500 nm (indexation of the observed characteristic reflections is shown in Fig. S6).<sup>51</sup> Moreover, our findings reveal that the HA formation is not limited to the materials surface, in contrast with conventional BG<sup>52, 53</sup> where a bone-like surface layer coats the material; here after 3 days soaking in SBF HA formation is extended to the entire SiO<sub>2</sub>-CaO/gelatin hybrid scaffold walls. For shorter immersion periods, small HA nanocrystals uniformly distributed throughout the scaffolds sections were observed, illustrating the high reactivity of these hybrids and the homogeneity of HA nucleation. This is obviously due to the highly disordered structures (low degree of condensation) of hybrids and the homogeneity of Ca incorporation as evidenced by NMR.

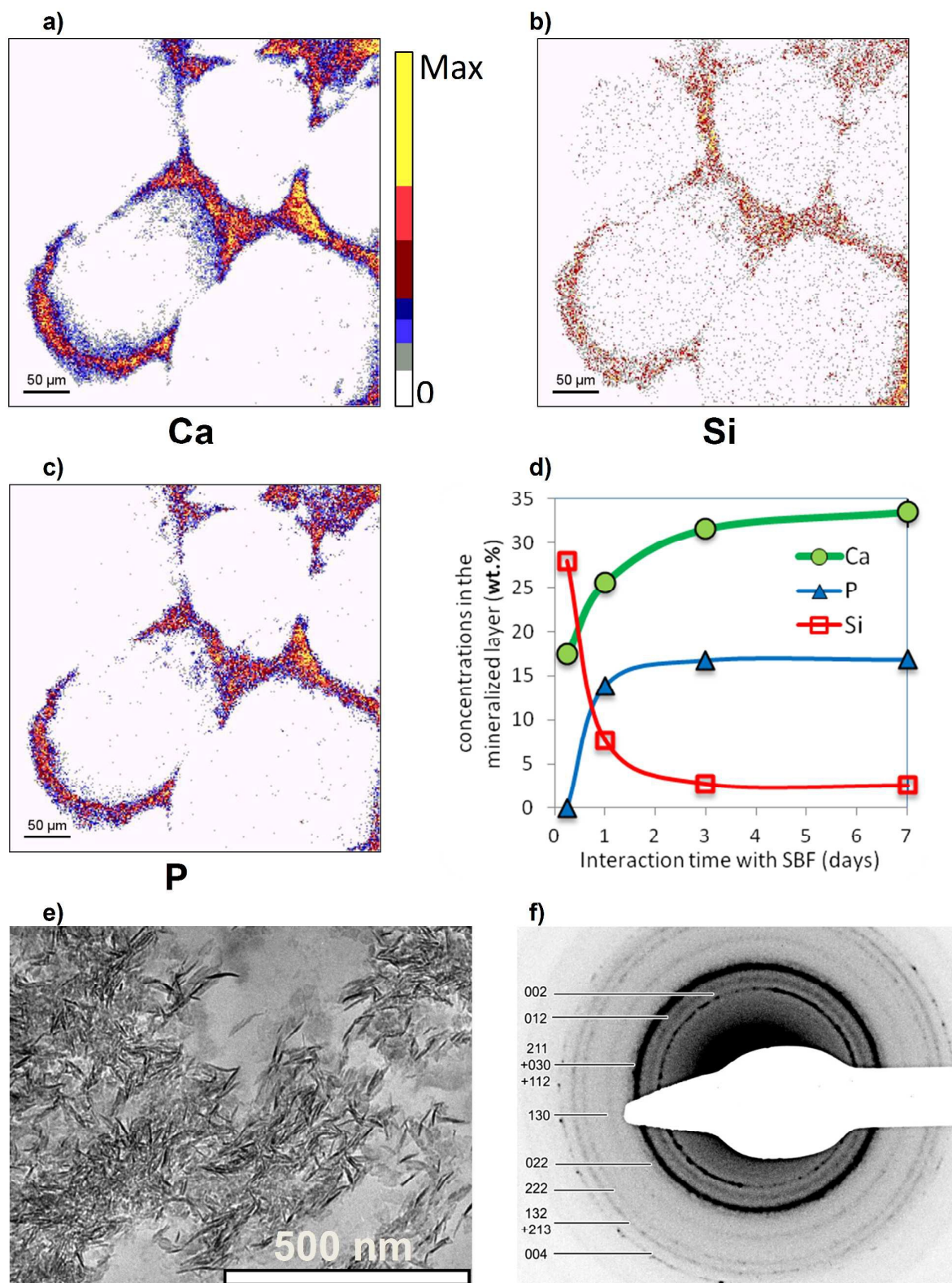
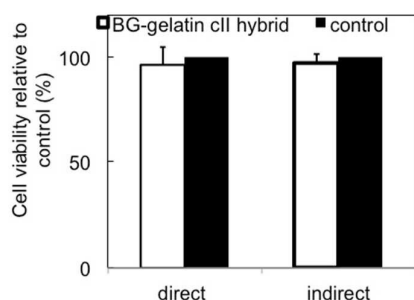


**Figure 6. Microanalysis of the mineralization process inside class II hybrid scaffolds (30wt.% SiO<sub>2</sub>-CaO/70 wt.% gelatin) using PIXE nuclear microprobe and TEM. a – c) PIXE quantitative chemical imaging of Ca, Si, P inside the cross-section of a class II hybrid scaffold after 3 days of interaction with Simulated Body Fluids. d) Evolution of Si, Ca, P concentrations in the mineralized areas of the scaffold as determined by PIXE with increasing**

time of interaction with SBF. Initial composition of the inorganic part of the hybrid is 75 wt.% SiO<sub>2</sub> – 25 wt.% CaO. **e**) TEM image (x 22,000 magnification) of a cross-section of class II gelatin/SiO<sub>2</sub>-CaO hybrid scaffolds after 3 days immersion in SBF, **f**) corresponding electron diffraction pattern showing the presence of HA nanocrystals (characteristic reflections of the HA hexagonal structure are indicated).

Finally the biocompatibility of class II BG-gelatin hybrids was investigated following the ISO 10993-5 procedure. In the literature, hybrids or composites biomaterials are systematically investigated after a long preincubation or washing step,<sup>8, 10, 15, 18, 19, 54</sup> which obviously can cause important chemical modifications (such as dealkalinization, ionic leaching or calcium phosphate precipitation) as BG are highly reactive towards biological fluids. The obtained results are therefore biased since the observed cellular responses do not correspond to the original raw material that is supposed to be implanted. To avoid this, here BG-gelatin hybrids were pre-incubated in biological medium for the shortest period of time (30 minutes, to be compared with several hours or even days in references<sup>8, 10, 15, 18, 19, 54</sup>). L929 murine fibroblast cell lines were then put in contact with hybrids. Results are presented in Figure 6 and demonstrate that BG-gelatin hybrids are non cytotoxic: cell viability is identical to that of the control conditions, no statistical differences being observed between the samples either in direct or in indirect cytotoxicity assays. BG-gelatin hybrids are thus demonstrated to be biocompatible.

**Figure 7. Direct and indirect cytotoxicity of class II BG-gelatin hybrids (30wt.% SiO<sub>2</sub>–CaO/70 wt.% gelatin).** For direct cytotoxicity assessment, L929 murine fibroblasts were put in contact with BG-gelatin hybrids for 24h. Solidified Agar was used as a control. For indirect cytotoxicity assessment, cells were placed opposite to BG-gelatin hybrids pellets and left for interaction for 2h. In this case control conditions correspond to absence of material. Differences between sample and control were estimated using non parametric Mann-Whitney tests (significance level was set to 0.05). Here differences are non significant.



### 3. Conclusion

Promising perspectives arise from the overall remarkable properties of these BG-gelatin hybrid scaffolds. Their synthesis remains noticeably simple relative to previous works requiring the use of inert atmospheres or harmful solvents<sup>14,23</sup> and the employed reactants and solvents generate safe by-products with no or only slight cytotoxicity. The process is readily upscalable for industrial production and its adaptability allows easy-shaped macroporous implant (see Fig. S8) with tailored pore sizes and interconnections to be made. Mechanical properties of the scaffolds under compression are similar to those of trabecular bones having the same porosity and these materials exhibit an apatite-forming ability even higher than that of pure SiO<sub>2</sub>-CaO BG foams having the same inorganic composition.<sup>55,56</sup> A key advantage is the HA formation is not limited to the surface; it is *the entire hybrid* which is progressively changed into bone-like minerals. Due to their adequate mechanical properties and their enhanced ability to form bone mineral, these materials can stand as competitive candidates for advanced applications in bone regenerative medicine and tissue engineering.

### 4. Materials and methods

**BG-gelatin hybrid sol synthesis:** BG oligomer solutions were obtained using TEOS (Aldrich, 99% purity) and calcium ethoxide (ABCR) precursors. TEOS is first hydrolysed in ethanol ethanol (absolute 99.8%, Aldrich) containing 2M HCl (obtained from 37% fuming, Aldrich) (volume ratio EtOH:HCl = 6:1 and molar ratio EtOH:TEOS = 6:1). A same volume of pure is used for the dilution of calcium ethoxide and the two solutions are mixed together to obtain a sol (containing all the glass precursors at a 12.65 wt% ratio) which is left for condensation for 1 hour. In parallel, a gelatin (type B, 225 g bloom number, Aldrich) aqueous solution is prepared and mixed with the inorganic sol for several minutes for homogenisation and further condensation. For the synthesis of class-II hybrid scaffolds, gelatin is first functionalized with 3-glycidoxypropyltrimethoxysilane (GPTMS, from ABCR) in a 12.65

wt.% aqueous solution containing 10 mM HCl (grafting between the epoxy end-group of GPTMS and the carboxylic acid groups of gelatin).<sup>57,58</sup> After hydrolysis of the GPTMS methoxysilane groups, the polymer solution is added to the sol to undergo condensation with the silanol groups of the glass oligomeric species.

**Scaffold synthesis:** the obtained hybrid sols are then poured onto a compact stack of PMMA microspheres (Kisker Biotech) in polyethylene moulds, and centrifugated at 6000 rpm. Gelation and ageing of the materials is performed at room temperature for 24 hours. The materials are immersed in acetone for 24 hours to dissolve the PMMA porogen spheres. This operation is renewed two times. Finally, the obtained macro porous hybrid scaffolds are dried in an oven at 40°C for 24 hours. For both class I and II hybrids, the inorganic compositions of the scaffolds measured by SEM-EDS are close to the expected values (Table S2).

5. Characterization **<sup>29</sup>Si solid state NMR** was used to validate calcium incorporation inside BG network and successful GPTMS grafting. All solid-state NMR experiments were performed on a Bruker Avance I spectrometer operating at a magnetic field of 9.4 T (<sup>1</sup>H and <sup>29</sup>Si Larmor frequencies of 400.2 and 79.5 MHz) using a 7 mm double resonance MAS probehead. The <sup>29</sup>Si quantitative MAS spectra were recorded at a spinning frequency of 6 kHz with a pulse duration of 1 μs (corresponding to a flip angle of 30°) and a recycle delay of 10s. The <sup>29</sup>Si-<sup>1</sup>H cross-polarization (CP) MAS spectra were acquired at a spinning frequency of 6 kHz with <sup>1</sup>H and <sup>29</sup>Si nutation frequencies of 62 and 48 kHz during the CP time, respectively and a recycle delay of 1s. In all case <sup>1</sup>H decoupling was applied during acquisition. The <sup>29</sup>Si through-space 2D homonuclear double quantum – single quantum MAS spectrum was recorded using the pulse sequence sketched in Figure S8. <sup>29</sup>Si longitudinal magnetization was first created by a <sup>1</sup>H-<sup>29</sup>Si CP block followed by a <sup>29</sup>Si 90° pulse. <sup>29</sup>Si double quantum (DQ) coherences were then excited and reconverted after an evolution period  $t_I$  using the BaBa-xy16 dipolar recoupling sequence.<sup>59</sup> A z-filter delay was applied before the final 90° read pulse. <sup>1</sup>H decoupling was applied during both the DQ excitation/reconversion periods and

signal acquisition.  $^{29}\text{Si}$  chemical shifts were referenced relative to TMS. Further experimental details are given in SI.

**In vitro bioactivity assay in SBF** allowed estimation of apatite-forming ability and degradation kinetics of BG-gelatin hybrids. The ISO-23317 standard procedure was followed. Briefly, c- SBF2, a protein-free solution of inorganic composition close to human blood plasma, was prepared following recommendations of Bohner et al <sup>36</sup>. Hybrid scaffolds were immersed in SBF at a 1 mg/mL ratio for up to 7 days at a constant temperature of 37°C. After interaction, aliquots of the solution are used for determination of the fluids composition by ICP-AES and gelatin dissolution measurements, while the scaffolds are carefully rinsed with pure ethanol and dried to avoid further mineralization reactions.

**Gelatin dissolution measurements.** Protein concentration in extracts of SBF were evaluated using a  $\mu$ -BCA protein assay kit (Thermo Scientific), which uses bicinchoninic acid (BCA) to monitor the reduction of alkaline  $\text{Cu}^{2+}$  by proteins (here gelatin). The gelatin concentration is deduced from the absorbance of the solution at 562 nm, measured using a UV-visible spectrophotometer, after calibration using standard solutions.

**PIXE nuclear microprobe analysis** is a technique very similar to SEM-EDS or electron microprobe, but has an increased 10 times sensitivity (at least). It was used here to visualize the chemical changes occurring inside BG-gelatin hybrid scaffolds during interaction with SBF. After interaction with SBF, the dried hybrid scaffolds were embedded in resin (AGAR, Essex, England) and 40  $\mu\text{m}$  cross-sections were cut using a LEICA RM 2145 microtome. PIXE (Particle-Induced X-ray Emission) quantitative microanalysis of the cross-sections was carried out at the AIFIRA platform (CENBG, France) using a 3 MeV incident proton beam (beam diameter of 1  $\mu\text{m}$ ). An 80  $\text{mm}^2$  Si (Li) detector (equipped with a 12  $\mu\text{m}$ -thick beryllium window and an aluminium funny filter with a tiny hole of 2 mm) orientated at 135° with respect to the incident beam axis was used for X-ray detection. Quantification was done

using the Gupixwin software after calibration against NIST 620 (soda-lime glass) standard reference material.

**Transmission Electron Microscopy** was conducted to characterize the formation of apatite nanocrystals inside BG-gelatin hybrids during interaction with SBF. 100 nm ultrathin cross-sections of materials were cut using a LEICA EM UC6 with diamond knives. A Phillips CM 20 microscope (LaB<sub>6</sub> thermoelectronic gun) operating at 200 kV was used to study the microstructure and morphology of hybrid scaffolds after soaking in SBF. The images were recorded with a Keenview CCD camera with 18.67 μm pixel size, and processed with the analySIS software. Home standards were used for calibration, and the SAED diffraction patterns were analyzed using ImageJ and CaRine softwares.

**Mechanical testing.** Mechanical properties of the scaffolds were measured under compression on cylindrical samples (diameter = height = 10 mm) using a UTS testing machine, equipped with a 50 kN-load cell and circular plates, at a crosshead speed of 0.5 mm/min. The elastic modulus was determined from the slope of the stress-strain curve over a range up to 2–3 % strain. The yield strength was determined using the 0.2% strain offset method. Measurements were also performed on wet scaffold samples, preliminary immersed in SBF at 37°C for 10 minutes, at a compression rate of 1N/min using a TA Instruments 2980 Dynamic Mechanical Analyser.

**Porosity calculation.** Pore diameters and interconnections were extracted from SEM pictures thanks to the Image J software. This method of measurement is here preferable to traditional mercury intrusion porosimetry which is limited to the characterization of pores under 250 μm.<sup>60</sup> Total porosity of the scaffolds was deduced from apparent density of cylindrical scaffolds of measured weights and dimensions and from gas pycnometry measurements (1.5 g/cm<sup>3</sup> scaffold skeletal density) using the formula: %porosity = (1 -  $d_{\text{apparent}}/d_{\text{skeletal}}$ ).

**Thermal characterizations** (Differential Scanning Calorimetry – DSC – and ThermoGravimetric Analysis – TGA) were used to evidence the successful grafting of GPTMS on both gelatin and BG chains in view of obtaining covalently bonded organic-inorganic networks. For DSC experiments, aluminium hermetic pans and lids were used for sample encapsulation. To prepare sealed hermetic pans, ca. 5 mg of sieved hybrid powders in the 50-100  $\mu\text{m}$  granulometric fraction was placed in the pan, which was then placed on a standard DSC press equipped with a hermetic sealing die. Once the lid was crimped in place, the pan was sealed off using the press. DSC experiments were performed by heating the sample from 0 to 250  $^{\circ}\text{C}$  under nitrogen atmosphere on a TA Instruments 2920 DSC instrument at a ramp rate of 5 $^{\circ}\text{C}/\text{min}$ . From the obtained thermograms, a second-order glass transition was visible and the temperature of glass transition was defined as the onset point of step-change in the specific heat of the sample. At higher temperature a first-order large endothermic transition was also visible and the temperature of the peak maximum was extracted.

TGA experiments were conducted on 10 mg of sieved hybrid powders in the 50-100  $\mu\text{m}$  granulometric fraction. Samples were placed in platinum pans and heated under nitrogen atmosphere at a ramp rate of 5 $^{\circ}\text{C}/\text{min}$  using a TA Instruments TGA2050 apparatus.

**Cytotoxicity tests.** The ISO 10993-5 procedure was followed in detail. Cytotoxicity was investigated using L929 mouse fibroblast cells as recommended by the procedure. Prior to testing, BG-gelatin hybrid scaffolds were pressed into 2 mm diameter pellets and sterilized through beta- irradiation. They were then incubated in culture medium at 0.1g/mL concentrations at 37 $^{\circ}\text{C}$  for the minimal period of time (30 minutes) to prevent chemical modifications of hybrids (such as dealkalinization or calcium phosphate precipitation) as they are highly reactive when in contact with biological fluids. L929 cells were seeded on 0.40  $\mu\text{m}$  filter at a 80,000 cells/mL concentration, let for 1h sedimentation and then put in contact with the materials. For direct cytotoxicity assessment, the cells were put in direct contact with 3.2

mm<sup>2</sup> BG-gelatin hybrid pellets for 24h. 10g/L solidified Agar was used as a control material. For indirect cytotoxicity assessment, the filter containing the cells were placed opposite to BG-gelatin hybrid pellets and left for interaction for 2h. In this case, the control conditions correspond to the absence of material. After interaction, the filters are removed and the cells are stained with Cresyl violet, then dissolved in acetic acid. The optical density of the obtained solution is measured through spectrophotometry and is a direct measurement of cell viability.

All experiments were repeated six times. Results of the six experiments are expressed as the mean  $\pm$  standard deviation and normalized against control conditions. Differences between sample and control were estimated using non parametric Mann-Whitney tests and were considered significant when  $p < 0.05$ .

### Electronic Supplementary Information

**Figure S1.** SEM images of class-I BG/gelatin hybrid scaffolds with 30 wt.% SiO<sub>2</sub>-CaO glass / 70 wt.% gelatin.

**Figure S2.** Experimental  $\{^1\text{H}\}$ -<sup>29</sup>Si CP MAS spectra of the class-I hybrids with 50 wt.% SiO<sub>2</sub>-CaO / 50 wt.% gelatin.

**Figure S3.** Experimental  $\{^1\text{H}\}$ -<sup>29</sup>Si CP MAS spectra of class-II hybrids with 50 wt.% SiO<sub>2</sub>-CaO / 50 wt.% gelatin.

**Figure S4.** Variation of the individual Q<sup>n</sup> and T<sup>n</sup> <sup>29</sup>Si resonance as a function of the CP duration for (a) class-I and (b) class-II hybrids with 50 wt.% SiO<sub>2</sub>-CaO / 50 wt.% gelatin.

**Figure S5:** TGA thermograms of type B gelatin and of pure SiO<sub>2</sub>-CaO sol-gel bioactive glass.

**Table S1.** Isotropic chemical shifts, linewidths and relative intensities of the Q<sup>n</sup> and T<sup>n</sup> resonances in class-I and class-II bioactive glass/gelatin hybrids (50 wt.% BG / 50 wt.% gelatin).

**Figure S6.** TEM images of different cross-sections of class II hybrid scaffolds (30wt.% SiO<sub>2</sub>-CaO/70 wt.% gelatin) after 3 days immersion in SBF and corresponding SAED pattern with detailed indexation.

**Figure S7.** Example of macroscopic shapes allowed for the BG/gelatin hybrid scaffolds.

**Table S2.** Inorganic compositions of BG hybrid scaffolds (30wt.% SiO<sub>2</sub>-CaO/70 wt.% gelatin) measured by SEM-EDS.

**Figure S7.** Pulse sequence used for the <sup>29</sup>Si homonuclear dipolar double quantum-single quantum correlation MAS experiment.

**Acknowledgements**

The Conseil Régional d'Auvergne is acknowledged for funding ("New Researcher" grant).

The SATT Grand-Centre is acknowledged for financial support.

Dr Fabrice Audonnet is deeply acknowledged for fruitful discussion of DSC thermograms.

Dr Mhammed Benbakkar and the Laboratoire Magma et Volcans (UMR 6524,

CNRS/Université Blaise Pascal) are acknowledged for ICP-AES measurements.

The Centre d'Etudes Nucléaires de Bordeaux-Gradignan and the AIFIRA staff are

acknowledged for allowing the PIXE experiments.

## REFERENCES

1. M. N. Rahaman, D. E. Day, B. Sonny Bal, Q. Fu, S. B. Jung, L. F. Bonewald and A. P. Tomsia, *Acta Biomater.*, 2011, **7**, 2355-2373.
2. J. R. Jones, *Acta Biomater.*, 2013, **9**, 4457-4486.
3. J. J. Blaker, A. Bismarck, A. R. Boccaccini, A. M. Young and S. N. Nazhat, *Acta Biomater.*, 2010, **6**, 756-762.
4. B. M. Novak, *Adv. Mater.*, 1993, **5**, 422-433.
5. S. Maeno, Y. Niki, H. Matsumoto, H. Morioka, T. Yatabe, A. Funayama, Y. Toyama, T. Taguchi and J. Tanaka, *Biomaterials*, 2005, **26**, 4847-4855.
6. P. J. Marie, *Bone*, 2010, **46**, 571-576.
7. S. Lin, C. Ionescu, K. J. Pike, M. E. Smith and J. R. Jones, *J. Mater. Chem.*, 2009, **19**, 1276-1282.
8. H. S. Costa, A. A. P. Mansur, M. M. Pereira and H. S. Mansur, *J. Nanomater.*, 2012, **2012**, 1-16.
9. C. Gao, Q. Gao, Y. Li, M. N. Rahaman, A. Teramoto and K. Abe, *J. Appl. Polym. Sci.*, 2013, **127**, 2588-2599.
10. L. Ren, K. Tsuru, S. Hayakawa and A. Osaka, *J. Sol-Gel Sci. Technol.*, 2003, **26**, 1137-1140.
11. L. L. Hench, *J. Eur. Ceram. Soc.*, 2009, **29**, 1257-1265.
12. M. M. Pereira, A. E. Clark and L. L. Hench, *J. Biomed. Mater. Res.*, 1994, **28**, 693-698.
13. A. Ramila, F. Balas and M. Vallet-Regi, *Chem. Mater.*, 2002, **14**, 542-548.
14. G. Poologasundarampillai, B. Yu, J. R. Jones and T. Kasuga, *Soft Matter*, 2011, **7**, 10241-10251.
15. B. Lei, K.-H. Shin, D.-Y. Noh, I.-H. Jo, Y.-H. Koh, W.-Y. Choi and H.-E. Kim, *J. Mater. Chem.*, 2012, **22**, 14133-14140.
16. O. Mahony, O. Tsigkou, C. Ionescu, C. Minelli, L. Ling, R. Hanly, M. E. Smith, M. M. Stevens and J. R. Jones, *Adv. Funct. Mater.*, 2010, **20**, 3808-3808.
17. O. Mahony, S. Yue, C. Turdean-Ionescu, J. Hanna, M. Smith, P. Lee and J. Jones, *J. Sol-Gel Sci. Technol.*, 2014, **69**, 288-298.
18. T. Qu and X. Liu, *J. Mater. Chem. B*, 2013, **1**, 4764-4772.
19. G. Poologasundarampillai, B. Yu, O. Tsigkou, D. Wang, F. Romer, V. Bhakhri, F. Giuliani, M. M. Stevens, D. S. McPhail, M. E. Smith, J. V. Hanna and J. R. Jones, *Chem. - Eur. J.*, 2014, **20**, 8149-8160.
20. J. Lao, J. Lacroix, J. Nohra, N. Naaman, J. M. Sautier and E. Jallot, *Surf. Interface Anal.*, 2014, **46**, 702-706.
21. L. Solorio, C. Zwolinski, A. W. Lund, M. J. Farrell and J. P. Stegemann, *J. Tissue Eng. Regen. Med.*, 2010, **4**, 514-523.
22. X. Dieudonne, V. Montouillout, E. Jallot, F. Fayon and J. Lao, *Chem. Commun.*, 2014, **50**, 8701-8704.
23. B. Yu, C. A. Turdean-Ionescu, R. A. Martin, R. J. Newport, J. V. Hanna, M. E. Smith and J. R. Jones, *Langmuir*, 2012, **28**, 17465-17476.
24. J. Isaac, J. Nohra, J. Lao, E. Jallot, J.-M. Nedelec, A. Berdal and J.-M. Sautier, *Eur. Cells Mater.*, 2011, **21**, 130-143.
25. G. Falini, S. Fermani, E. Foresti, B. Parma, K. Rubini, M. C. Sidoti and N. Roveri, *J. Mater. Chem.*, 2004, **14**, 2297-2302.

26. A. Bigi, G. Cojazzi, S. Panzavolta, N. Roveri and K. Rubini, *Biomaterials*, 2002, **23**, 4827-4832.
27. I. Grizzi, H. Garreau, S. Li and M. Vert, *Biomaterials*, 1995, **16**, 305-311.
28. N. Sivadas, D. O'Rourke, A. Tobin, V. Buckley, Z. Ramtoola, J. G. Kelly, A. J. Hickey and S.-A. Cryan, *Int. J. Pharm.*, 2008, **358**, 159-167.
29. S. F. Hulbert, S. J. Morrison and J. J. Klawitter, *J. Biomed. Mater. Res.*, 1972, **6**, 347-374.
30. V. Karageorgiou and D. Kaplan, *Biomaterials*, 2005, **26**, 5474-5491.
31. M. Descamps, O. Richart, P. Hardouin, J. C. Hornez and A. Leriche, *Ceram. Int.*, 2008, **34**, 1131-1137.
32. M. Descamps, T. Duhoo, F. Monchau, J. Lu, P. Hardouin, J. C. Hornez and A. Leriche, *J. Eur. Ceram. Soc.*, 2008, **28**, 149-157.
33. S. Jung and J. Kleinheinz, in *Advances in Regenerative Medicine*, ed. S. Wislet-Gendebien, In Tech, 2011.
34. G. E. Maciel and D. W. Sindorf, *J. Am. Chem. Soc.*, 1980, **102**, 7606-7607.
35. P. Zhang, P. J. Grandinetti and J. F. Stebbins, *J. Phys. Chem. B*, 1997, **101**, 4004-4008.
36. M. Bohner and J. Lemaitre, *Biomaterials*, 2009, **30**, 2175-2179.
37. X. Lu and Y. Leng, *Biomaterials*, 2005, **26**, 1097-1108.
38. W. Lai, J. Garino and P. Ducheyne, *Biomaterials*, 2002, **23**, 213-217.
39. I. Mukherjee and M. Rosolen, *J. Therm. Anal. Calorim.*, 2013, **114**, 1161-1166.
40. L. T. Zhuravlev, *Colloids and Surfaces A: Physicochemical and Engineering Aspects*, 2000, **173**, 1-38.
41. L. J. Gibson, *J. Biomech.*, 2005, **38**, 377-399.
42. S. Callcut and J. C. Knowles, *J. Mater. Sci.: Mater. Med.*, 2002, **13**, 485-489.
43. Q. Fu, E. Saiz, M. N. Rahaman and A. P. Tomsia, *Mater. Sci. Eng., C*, 2011, **31**, 1245-1256.
44. A. J. Wagoner Johnson and B. A. Herschler, *Acta Biomater.*, 2011, **7**, 16-30.
45. T. M. Keaveny, E. F. Morgan and O. C. Yeh, in *Standard Handbook of Biomedical Engineering & Design*, ed. M. Kutz, McGraw-Hill Professional, 2003, pp. 221-243.
46. D. L. Kopperdahl and T. M. Keaveny, *J. Biomech.*, 1998, **31**, 601-608.
47. H. Follet, K. Bruyère-Garnier, F. Peyrin, J. P. Roux, M. E. Arlot, B. Burt-Pichat, C. Rumelhart and P. J. Meunier, *Bone*, 2005, **36**, 340-351.
48. I. Hvid, P. Christensen, J. R. Sondergaard, P. B. Christensen and C. G. Larsen, *Acta Orthop.*, 1983, **54**, 819-825.
49. S. A. Goldstein, *J. Biomech.*, 1987, **20**, 1055-1061.
50. S. V. Dorozhkin and M. Epple, *Angew. Chem. Int. Ed.*, 2002, **41**, 3130-3146.
51. E. I. Suvorova and P. A. Buffat, *J. Microsc.*, 1999, **196**, 46-58.
52. M. Vallet-Regí, C. V. Ragel and Antonio J. Salinas, *Eur. J. Inorg. Chem.*, 2003, **2003**, 1029-1042.
53. T. Kokubo, *Acta Mater.*, 1998, **46**, 2519-2527.
54. S. Midha, T. B. Kim, W. van den Bergh, P. D. Lee, J. R. Jones and C. A. Mitchell, *Acta Biomater.*, 2014, **9**, 9169-9182.
55. E. Jallot, O. Raissle, J. Soulie, J. Lao, G. Guibert and J.-M. Nedelec, *Adv. Eng. Mater.*, 2010, **12**, B245-B255.
56. J. Lacroix, E. Jallot, J.-M. Nedelec and J. Lao, *J. Phys. Chem. B*, 2013, **117**, 510-517.
57. L. Ren, K. Tsuru, S. Hayakawa and A. Osaka, *J. Sol-Gel Sci. Technol.*, 2001, **21**, 115-121.
58. O. Mahony, O. Tsigkou, C. Ionescu, C. Minelli, L. Ling, R. Hanly, M. E. Smith, M. M. Stevens and J. R. Jones, *Adv. Funct. Mater.*, 2010, **20**, 3835-3845.
59. K. Saalwächter, F. Lange, K. Matyjaszewski, C.-F. Huang and R. Graf, *J. Magn. Reson.*, 2011, **212**, 204-215.

60. J. R. Jones and L. L. Hench, *J. Mater. Sci.*, 2003, **38**, 3783-3790.